Metal Exchange of ZIF-8 and ZIF-67 Nanoparticles with Fe(II) for Enhanced Photocatalytic Performance

Lehlohonolo E. Mphuthi, Elizabeth Erasmus, and Ernst H. G. Langner*

ACCESS | Metrics & More | Article Recommendations | SI Supporting Information

ABSTRACT: Zeolitic imidazolate frameworks (ZIFs), such as ZIF-8 and ZIF-67, were found to be efficient catalysts. However, ZIFs are not used much in photocatalysis due to their low photocatalytic activity for most reactions. The photocatalytic activity can be improved by modifying the framework by exchanging the Zn(II) ions (ZIF-8) and Co(II) ions (ZIF-67) with a more photocatalytically active metal(II) ion to form an efficient bimetallic ZIF photocatalyst. Redox-active iron (Fe)-based materials are known to be highly potent photocatalysts. Thus, incorporating iron into ZIFs could significantly enhance their photocatalytic performance. In this study, we modified nanosized ZIF-8(Zn) and ZIF-67(Co) via metal (Fe^{2+}) exchange to produce bimetallic frameworks that are photocatalytically more active than their parent ZIFs. Nanosized ZIF-8 and ZIF-67 were synthesized isothermally in either water or methanol under ambient conditions. From these, Fe-containing bimetallic ZIF-8 and ZIF-67 nanoparticles were synthesized via the metal exchange, and their performance on the photocatalytic degradation of dye was evaluated. The morphology and crystal structures of the pristine ZIF-8 and ZIF-67 nanoparticles were retained to a large extent during the iron exchange. Their Brunauer−Emmett−Teller (BET) surface areas decreased by less than 15% for nZIF-8 and less than 12% for nZIF-67. The binding energy values on X-ray photoelectron spectroscopy (XPS) confirmed the preservation of the oxidation state of Fe(II) during the exchange process. A remarkably higher catalytic activity was observed for the photocatalytic degradation of dye by the Fe-exchanged nZIF-8 and nZIF-67 compared to their parent ZIFs. This proved that the incorporation of Fe(II) centers into the ZIF framework enhanced the photocatalytic activity of the framework dramatically. In addition, these catalysts can be regenerated and reused without an appreciable loss in activity.
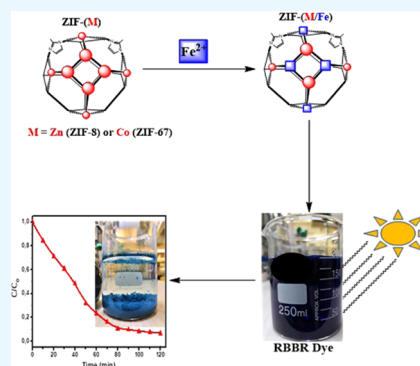
1. INTRODUCTION

Porous materials are an interesting and important class of materials that have attracted a great deal of attention because of their unique and desirable properties: high surface area and large and tunable pore sizes.[1,2] These extraordinary materials hold vast promise in several potential applications like gas separation and storage, chemical sensing, photocatalysis, biomedicine, and water treatment.[2−6] Metal−organic frameworks (MOFs), part of porous coordination polymers (PCPs), are crystalline porous hybrid materials comprising metal ions, bridged by organic molecules. They can be synthesized from a wide range of metal ions and organic linkers.[7,8]

Zeolitic imidazolate frameworks (ZIFs) are an emerging subfamily of MOFs that primarily comprise metal ions, linked by imidazolate derivatives.[9] ZIF-8 is the most commonly researched ZIF, as it is easy to synthesize and reproduce. It is mainly composed of Zn^{2+} ions and 2-methylimidazolate (2-MeIm) linkers and has a sodalite (SOD) topology.[10−13] ZIF-67(Co),[14] Mg(Meim)$_2$,[15] CdIF-1,[16] Mn(Meim)$_2$,[17] and the more recent Fe(Meim)$_2$[18] are identified as isostructural metal counterparts of ZIF-8. Despite their numerous potential applications, the interesting iron counterparts produced by Fe^{2+} centers have remained elusive for years. All attempts to adapt different synthetic solvent-based approaches of ZIF-8 or

ZIF-67 to Fe(II)-containing ZIFs, especially Fe(II) as metal centers in ZIFs, have been unfruitful.[18]

ZIFs hold vast promise in several potential applications, including catalysis.[19] However, ZIFs are not used much in photocatalysis due to their low photocatalytic activity for most reactions.[20] The photocatalytic activity of ZIFs can be improved using a very powerful approach called postsynthetic modification (PSM), which helps design materials for a specific application.[21] Metal ions in MOFs can be exchanged through the postsynthetic metal exchange. This method may be used to alter MOFs under ambient conditions.[22−25] The photocatalytic activity of ZIFs can be improved by modifying the framework by metal-ion exchange, exchanging the Zn(II) ions (ZIF-8) and Co(II) ions (ZIF-67) with a more photocatalytically active metal(II) ion to form an efficient bimetallic ZIF photocatalyst. Redox-active iron (Fe)-based materials are known to be highly
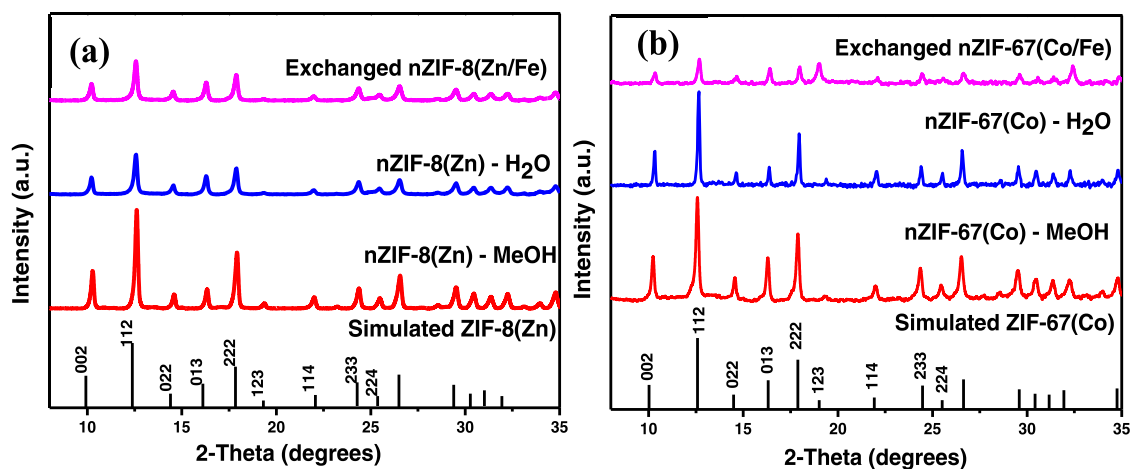
A

Figure 1. PXRD patterns of (a) nZIF-8(Zn) with nZIF-8(Zn/Fe) and (b) nZIF-67(Co) with nZIF-67(Co/Fe) synthesized in methanol (MeOH) and deionized water (H$_2$O).
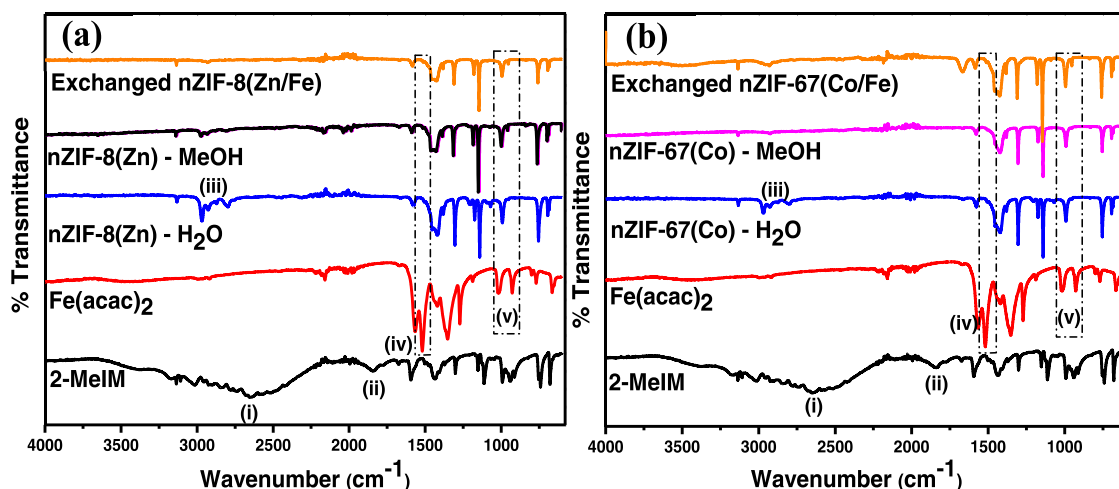

Figure 2. FTIR spectra of (a) nZIF-8(Zn) with nZIF-8(Zn/Fe) and (b) nZIF-67(Co) with nZIF-67(Co/Fe) synthesized in methanol (MeOH) and deionized water (H$_2$O).

potent photocatalysts.[18,26] Thus, incorporating iron into ZIFs could significantly enhance their photocatalytic performance.

The primary focus of this paper is on the modification of nano-ZIF-8(Zn) and nano-ZIF-67(Co) particles via metal (Fe^{2+}) exchange to produce bimetallic frameworks that are photocatalytically more active than their parent ZIFs. A redox-active metal, Fe^{2+}, is incorporated as a metal center in nZIF-8(Zn) and nZIF-67(Co) nanoparticles without causing structural changes to enhance the photocatalytic activity of the frameworks.

2. RESULTS AND DISCUSSION

ZIF nanoparticles were synthesized using a rapid isothermal benchtop reaction utilizing methanol and deionized water as solvents. The reaction commenced with the deprotonation of 2-methylimidazole (2-MeIM), which coordinated to the Zn(II) or Co(II) ions in a tetrahedral manner to form nZIF-8(Zn) or nZIF-67(Co) crystallites, respectively. An excess of 2-methylimidazole ligand and PVP-10 shielded the particles from further growth, leading to the formation of nanoparticles. Triethylamine (TEA) was used to accelerate the deprotonation of 2-MeIm to reduce the molar ratio of metal ion to an organic ligand and thus to promote the formation of nanosized ZIFs.

Fe(acac)$_2$ was employed as a source of Fe(II) to partially substitute Zn^{2+} (ZIF-8) and Co^{2+} (ZIF-67), coordinating to 2-MeIM in a tetrahedral manner, resulting in the formation of bimetallic nZIF-8(Zn/Fe) or nZIF-67(Co/Fe) crystallites. The presence of Fe(II) in nZIF-8 and nZIF-67 was confirmed by scanning electron microscopy–energy-dispersive X-ray spectroscopy (SEM–EDX), X-ray photoelectron spectroscopy (XPS), and inductively coupled plasma-optical emission spectroscopy (ICP-OES).

The preservation of the structural integrity of nZIF-8 and nZIF-67 during the metal exchange with Fe(II) was demonstrated by the similar powder X-ray diffraction (PXRD) patterns of pristine nZIF-8 or nZIF-67 nanoparticles and their iron-exchanged derivatives (Figure 1). The well-defined PXRD patterns of all ZIFs synthesized in methanol and water confirmed their crystallinity and sodalite (SOD) topologies, which, again in both cases, showed similar patterns and were in good agreement with the simulated pattern.[10−14] The peak intensity of the Fe-exchanged ZIFs decreased slightly as compared to those of the parent ZIFs, suggesting a minor loss of crystallinity during the metal exchange, which might be attributed to the preferred octahedral coordination of Fe(II) being forced into tetrahedral coordination during the metal
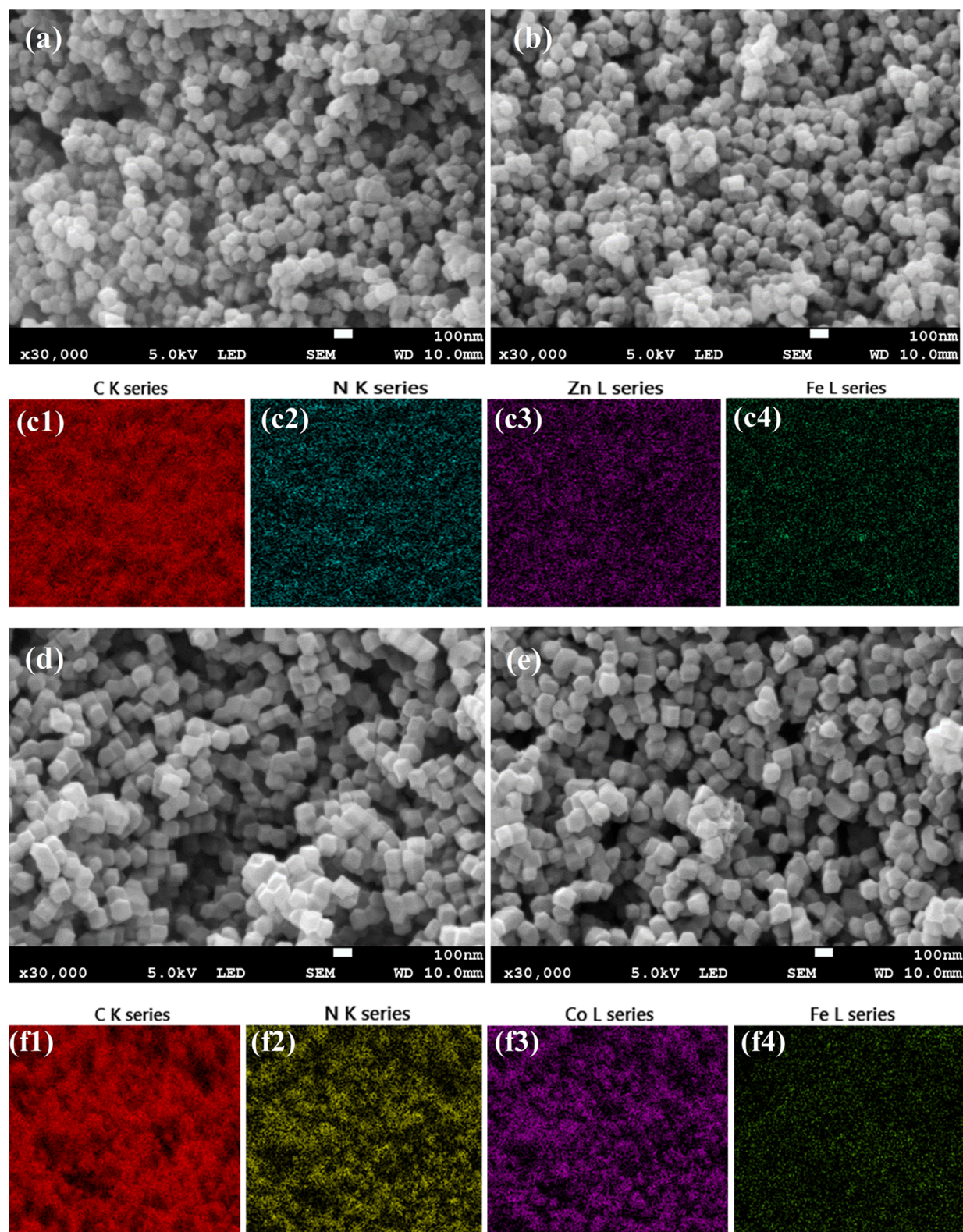
Figure 3. SEM images of (a) ZIF-8(Zn), (b) nZIF-8(Zn/Fe), (d) nZIF-67(Co), (e) nZIF-67(Co/Fe), and EDX mapping of Fe-exchanged nZIF-8(Zn/Fe) (c1−c4) and nZIF-67(Co/Fe) (f1−f4) synthesized in methanol.

exchange.[23,31] The preserved SOD topology and structural integrity imply tetrahedral coordination for all metal ions, including exchanged Fe(II). These results show that nZIF-8 and nZIF-67 are relatively stable, and the crystal structures have been retained to a large extent during the exchange with Fe(II).

Fourier transform infrared spectroscopy (FTIR) was used to confirm that the obtained nZIF-8, nZIF-67, and the Fe-exchanged ZIF materials contained no unreacted precursors. The FTIR spectrum of 2-methylimidazole (2-MeIm) (Figure 2) shows a strong broad peak between 2200 and 3300 cm^{-1} (i), which is associated with N−H stretching. The resonance of

C

Table 1. XPS Data and Binding Energies of ZIF-8, ZIF-67 and Their Fe-Exchanged Derivatives

	N	Zn		Co(main)		Co(sat)		Fe(main)		Fe(sat)	
	1s	2p$_{3/2}$	2p$_{3/2}$	2p$_{3/2}$	2p$_{3/2}$	2p$_{3/2}$	2p$_{3/2}$	2p$_{3/2}$	2p$_{3/2}$	2p$_{3/2}$	2p$_{3/2}$
ZIF-8-(Zn)	398.8	1021.9	1045.0								
atomic ratio	1	0.51									
ZIF-67-(Co)	398.7			780.8	797.1	785.7	803.2				
atomic ratio	1			0.46							
ZIF-8-(Zn/Fe)	398.8	1021.6	1044.7					710.9	724.5	717.9	731.5
atomic ratio	1	0.40						0.13			
ZIF-67-(Co/Fe)	399.0			781.2	797.4	785.8	803.1	711.0	724.9	717.7	731.3
atomic ratio	1			0.33				0.09			

N−H out-of-plane bending is found at 1843 cm^{-1} (ii). These vibrations are completely absent from the spectra of both nZIF-8 and nZIF-67 and those of the Fe-exchanged ZIFs, indicating the deprotonation of the N−H groups of the 2-MeIm ligands upon coordination with Zn^{2+} or Co^{2+} ions. It can be deduced from the absence of those bands that there is no unreacted 2-MeIm in all synthesized ZIF materials.

All of the iron-exchanged ZIF materials, nZIF-8(Zn/Fe) and nZIF-67(Co/Fe), exhibit FTIR spectra comparable to that of the pristine nZIF-8(Zn) and nZIF-67(Co), respectively, as seen in Figure 2. Compounds synthesized with deionized water show hydroxylated aromatic compounds that are produced from free hydroxyl (−OH) groups that react with the organic ligands (iii).[28] FTIR spectra of both Fe-exchanged ZIFs with Fe(acac)$_2$ were compared to monitor the removal of unreacted Fe(acac)$_2$ from the products. The characteristic bands for Fe(acac)$_2$ are highlighted: (iv) 1565 cm^{-1} (C−O stretch vibration) and (v) 1018 and 928 cm^{-1}. The absence of those bands in the spectra of ZIFs after exchange reaction strongly indicates the absence of unreacted Fe(acac)$_2$ in the Fe-exchanged products. Also, no additional bands, compared to the parent ZIFs, are observed, indicating that no additional bonds are present after the exchange reaction.

The morphologies of the parent and Fe-exchanged ZIFs, as well as the dispersity of Fe(II) in the exchanged products, were studied using SEM−EDX. The SEM pictures taken before (left) and after (right) the Fe exchange clearly show very little change in particle size and morphology of ZIFs (Figure 3). The SEM images of the nZIF-8 crystals (Figure 3a) show uniform and agglomerated nanosized structures, which is in strong agreement with the literature.[28−30] The particle size distribution was plotted for all ZIFs, and the average particle size (diameter in nm) was obtained (Supporting Information Figure S4). The average particle size of nZIF-8 is 52 nm (synthesized in methanol) and 65 nm (synthesized in water). The nZIF-67 crystals are larger than nZIF-8 crystals, averaging 109 nm (synthesized in methanol) and 124 nm (synthesized in water) (Figure 3d). The nanosized ZIF-67 crystallites were obtained using surfactants, shaping the micelles in an aqueous solution via their hydrophilic−hydrophobic interactions. SEM images of the ZIFs synthesized in deionized water are found in the Supporting Information, Figure S1. The SEM images of nZIF-8(Zn/Fe) and nZIF-67(Co/Fe) (Figure 3b,e) exhibit nanosized crystallites similar to the parent ZIFs, averaging 48 nm (nZIF-8(Zn/Fe)) and 106 nm (nZIF-67(Co/Fe)). The smallest particles were obtained with the synthesis in methanol. The EDX spectra obtained from the nanoparticles are presented in the Supporting Information, Figure S2. SEM−EDX mapping of Fe-exchanged ZIFs clearly shows a consistent and even distribution of C, N, Zn, Co, and Fe (Figure 3c,f),

which is quite similar to the EDX mapping of the parent ZIFs (Supporting Information, Figure S3). All elements are equally spread on the surface of the materials, as seen on the mapping, indicating that ion exchange can occur uniformly on the crystal surface.[25]

To further characterize the modified ZIF materials, nZIF-8(Zn/Fe) and nZIF-67(Co/Fe), X-ray photoelectron spectroscopy (XPS) measurements were collected to determine the composition, oxidation states of metals, and atomic ratios of elements present within the samples. The comparative XPS data of pristine nZIF-8(Zn) and nZIF-67(Co) with the Fe-exchanged nZIF-8(Zn/Fe) and nZIF-67(Co/Fe) are summarized in Table 1, and the N 1s, Co 2p, and Fe 2p XPS regions of nZIF-67(Co/Fe) as well as the Zn 2p region of nZIF-8(Zn/Co) are shown in Figure 4.

The maximum binding energy of carbon's C 1s photoelectron line was used as a charge reference, which was positioned at 284.8 eV.[26,32,35] All ZIF materials showed a symmetrical N 1s photoelectron line for the nitrogen atoms of the organic linker, with the binding energy located at ca. 398.9 eV (Figure 4a). The zinc-containing compounds nZIF-8(Zn) and nZIF-8(Zn/Fe) showed the Zn 2p$_{3/2}$ photoelectron line at binding energies of ca. 1022.1 eV, with a spin-orbit splitting of ca. 23.1 eV between the Zn 2p$_{3/2}$ and Zn 2p$_{1/2}$ (Figure 4d). The observed binding energies were compatible with Zn^{2+} of the ZIF-8 structure as reported.[26,33,34] For cobalt-containing nZIF-67(Co) and nZIF-67(Co/Fe) compounds, the XPS revealed the Co 2p$_{3/2}$ and the Co 2p$_{1/2}$ photoelectron line at ca. 780.8 and 797.1 eV, respectively (Figure 4b). These values correlated well with reported data.[34] A satellite structure was observed at ca. 4.9 eV higher than the main Co 2p$_{3/2}$ and Co 2p$_{1/2}$ photoelectron lines due to the shake-up mechanism. The intensity of the satellite to the main photoelectron lines was ca. 30%, with the intensity increasing after the metal-exchange reaction.

The observed Fe 2p$_{3/2}$ and Fe 2p$_{1/2}$ photoelectron lines at ca. 710.9 and 724.5 eV (Figure 4c), respectively, confirmed that the metal-exchange reaction did work. The binding energy values confirmed that Fe is present in an oxidation state of (II). Similar to Co, the Fe 2p$_{3/2}$ and Fe 2p$_{1/2}$ photoelectron lines showed a satellite structure at ca. 6.8 eV higher. The intensity of the satellite to the main photoelectron lines was ca. 30%. From the % atomic ratios, the success of the metal-exchange reaction was found to be 25 and 21% for nZIF-8(Zn/Fe) and nZIF-67(Co/Fe), respectively.

XPS and ICP-OES were used to determine the metallic content (Zn, Co, and Fe) of the materials. To determine the relative amount of Fe(II), inductively coupled plasma-optical emission spectroscopy (ICP-OES) was utilized after the digestion of the ZIF crystal materials in an aqueous solution
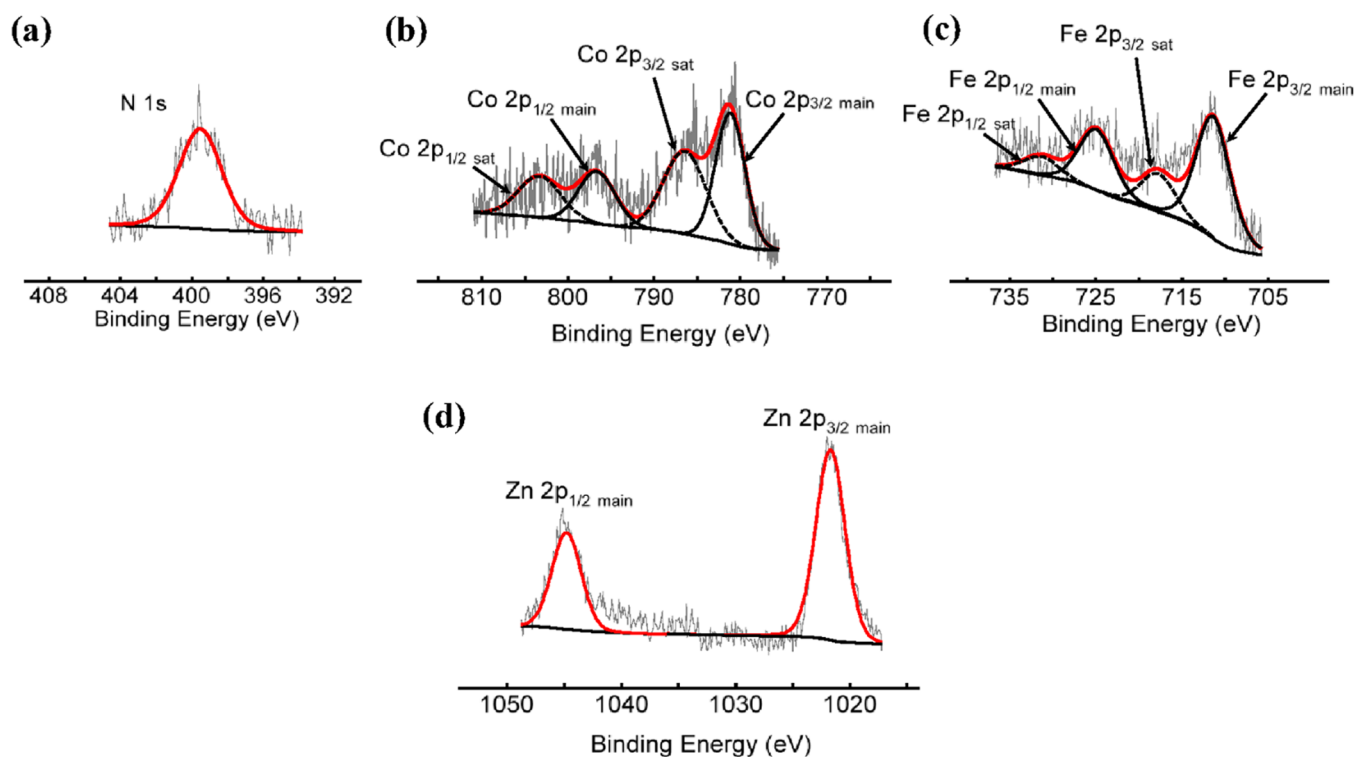
Figure 4. (a) N 1s, (b) Co 2p, and (c) Fe 2p XPS regions of nZIF-67(Co/Fe) [top row] as well as the (d) Zn 2p region of nZIF-8(Zn/Co) [bottom row].

of HNO₃. ICP-OES revealed that Fe/Zn ratio in nZIF-8(Zn/Fe) and Fe/Co ratio in nZIF-67(Co/Fe) were 0.376:1 and 0.295:1 (average of the three measurements), respectively, which are in good agreement with the values obtained by XPS (Table 2) for the same samples. From the molar ratios measured by ICP-OES, the Fe content was found to be 27 and 23% for nZIF-8(Zn/Fe) and nZIF-67(Co/Fe), respectively.

Table 2. Fe Content (mol %) of Exchanged ZIF Materials as Measured by XPS and ICP-OES

technique	nZIF-8 (Fe/Zn) mol %	nZIF-67 (Fe/Co) mol %
XPS	25	21
ICP-OES	27	23

All of the ZIF materials exhibit type I adsorption isotherms (Figure 5), indicating that all these materials are microporous.[10−14] The slight decrease in the amount of N₂ adsorbed as well as Brunauer−Emmett−Teller (BET) surface areas was observed for both nZIF-8 and nZIF-67 after the metal exchange with Fe(II) (Table 3). These marked decreases in surface areas and pore volumes are in good agreement with the decrease in crystallinity as shown by PXRD measurements (Figure 1), and what was reported by Thanh et al.,[26] when they increased the amount of Fe(II) doping on ZIF-8. The hysteresis loop in the N₂ desorption isotherm of nZIF-67, synthesized in water, can be attributed to capillary condensation of nitrogen in spaces between particles due to agglomeration.
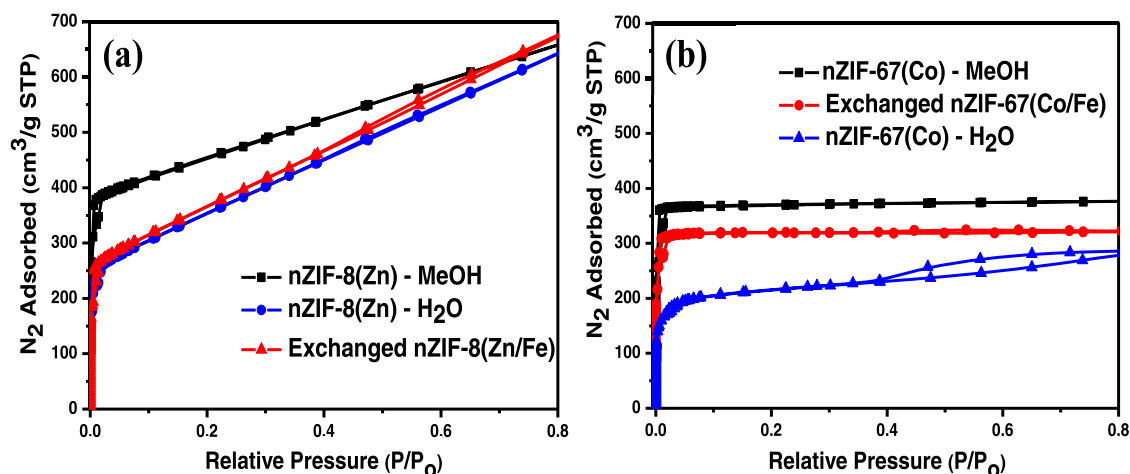

Figure 5. Nitrogen (N₂) adsorption isotherms of (a) nZIF-67(Co) with ZIF-67(Co/Fe) and (b) nZIF-8(Zn) with ZIF-8(Zn/Fe).

Table 3. Summary of Results for nZIF-8, nZIF-67, and Their Iron-Exchanged Derivatives

| sample	synthesis solvent	yield (%)	BET surface area (m^2 g^{-1})	average particle size (nm)	d_{pore} (Å)	V_{pore} (cm^3 g^{-1})	T_{decomp} (°C)	band gap energy (eV)
nZIF-8(Zn)	MeOH	63	1614	52	15.4	0.721	500	5.00
nZIF-8(Zn)	H$_2$O	94	1330	65	14.9	0.661	485	5.00
nZIF-8 (Zn/Fe)	MeOH	85	1397	48	14.5	0.546	450	5.01
nZIF-67(Co)	MeOH	61	1401	109	14.3	0.508	400	2.01
nZIF-67(Co)	H$_2$O	93	1211	124	13.9	0.481	370	2.01
nZIF-67 (Co/Fe)	MeOH	81	1255	106	12.5	0.419	350	2.02
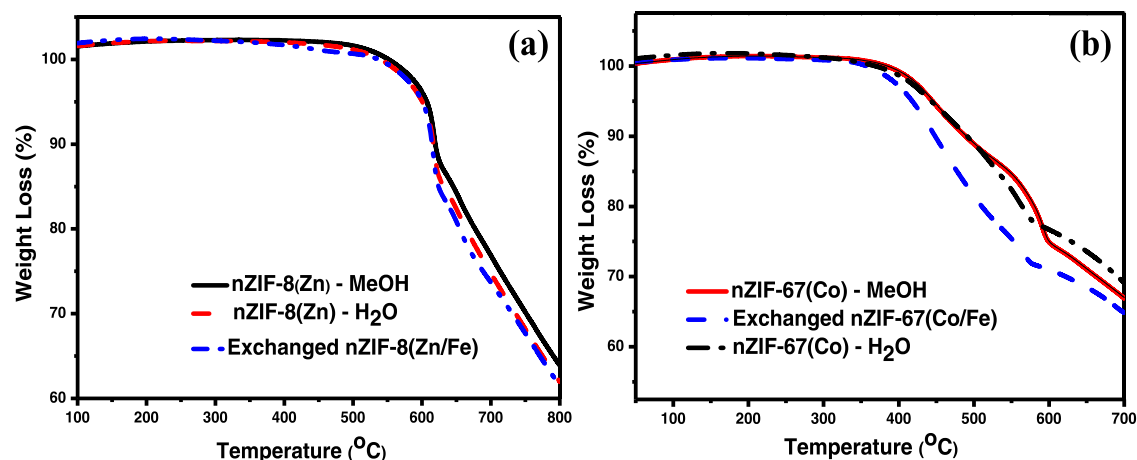
Figure 6. Thermogravimetric analysis (TGA) thermograms of (a) nZIF-8(Zn) with nZIF-8(Zn/Fe) and (b) nZIF-67(Co) with nZIF-67(Co/Fe) under N$_2$ atmosphere.

The thermal profiles of all ZIF materials are presented in Figure 6. nZIF-8 and its Fe-exchanged derivative show the highest thermal stability, up to 450 °C, while nZIF-67 and its Fe-exchanged derivative can tolerate temperatures to up to 350 °C. The thermal stability of both nZIF-8 and nZIF-67 decreased only slightly after the exchange reaction with Fe(II) (Table 3), consistent with the literature, where metal exchange generally reduces the thermal stability of the original framework.[31]

All Fe-exchanged ZIF samples were exposed to the atmosphere for several days to evaluate the stability of the compounds in air, since all Fe-exchanged ZIFs contain Fe(II), and Fe(II) is unstable in air. FTIR and XPS techniques were used to evaluate whether the samples went through oxidation or not. All of the exposed Fe-exchanged ZIFs exhibited FTIR spectra comparable to those of the original Fe-ZIFs. Also, no additional bands were observed, indicating that no additional bonds were present after exposing samples to the atmosphere for days. The observed Fe 2p$_{3/2}$ and Fe 2p$_{1/2}$ photoelectron lines at ca. 711.7 and 725.3 eV on XPS spectrum (Supporting Information, Figure S5), respectively, confirmed that no oxidation occurred for Fe-exchanged samples as the oxidation state of Fe(II) was intact. This strongly indicates that Fe-exchanged ZIFs are relatively stable.

The band gaps of nZIF-8, nZIF-67, and their Fe-Exchanged derivatives were determined by UV−vis absorption measurements at room temperature (Figure 7). All absorbance spectra had broad absorbance bands in the visible region. The curve of $(\alpha*E)^2$ versus E (where α is an absorption coefficient and E is the photon energy)[26] was plotted as shown in Figure 7. The band gap energies of all ZIF materials were determined by the extrapolation of the gradients to the x-axes (where $E = E_g$ (the apparent band gap energy)), and the results are shown in

Table 3. The absorbance peak of pristine nZIF-8(Zn) (300−360 nm) corresponded to a band gap of 5.00 eV (previous reports: 5.2 and 4.9 eV),[26,44] while the broad absorbance peak of Fe-exchanged nZIF-8(Zn/Fe) (320−700 nm) corresponded to a band gap of 5.01 eV. The very high absorbance around 230 nm involved $\pi \rightarrow \pi^*$ transitions in the imidazole rings.[26] The absorbance peak of nZIF-67 (500−650 nm) corresponded to an Eg of 2.01 eV (reported literature value: 1.98 eV),[44] with the Eg of Fe-exchanged nZIF-67(Co/Fe) at 2.02 eV.

3. PHOTOCATALYTIC APPLICATION

3.1. Photocatalytic Degradation of Remazol Brilliant Blue R (RBBR) Textile Dye. The photocatalytic activity of metal-exchanged nZIF-8(Zn/Fe) and nZIF-67(Co/Fe), compared to those of their parents nZIF-8 (Zn) and nZIF-67(Co), was studied using the decomposition of Remazol Brilliant Blue R (RBBR) dye under simulated sunlight irradiation. Remazol Brilliant Blue R is a harmful anthraquinone dye used in the textile industry. It is stable and does not decompose biologically due to the presence of aromatic rings.[36−38] RBBR dye degradation was carried out in both dark and photocatalytic conditions. To compare the removal efficiencies of RBBR dye, control experiments were carried out. The amount of nZIF-8, nZIF-67, nZIF-8(Zn/Fe), and nZIF-67(Co/Fe) catalysts used in each experiment was kept constant (50 mg). With an initial RBBR dye concentration of 20 mg dm^{-3} and a pH of 7.0, the effect of light and ZIF photocatalysts on the photocatalytic degradation of RBBR dye was evaluated (Scheme 1).

Figure 8 shows a comparison of the kinetics of dark adsorption and photocatalytic reaction after 120 min with UV−vis spectrum, the data is given in the Supporting Information, Figure S7. Photolysis tests, carried out under
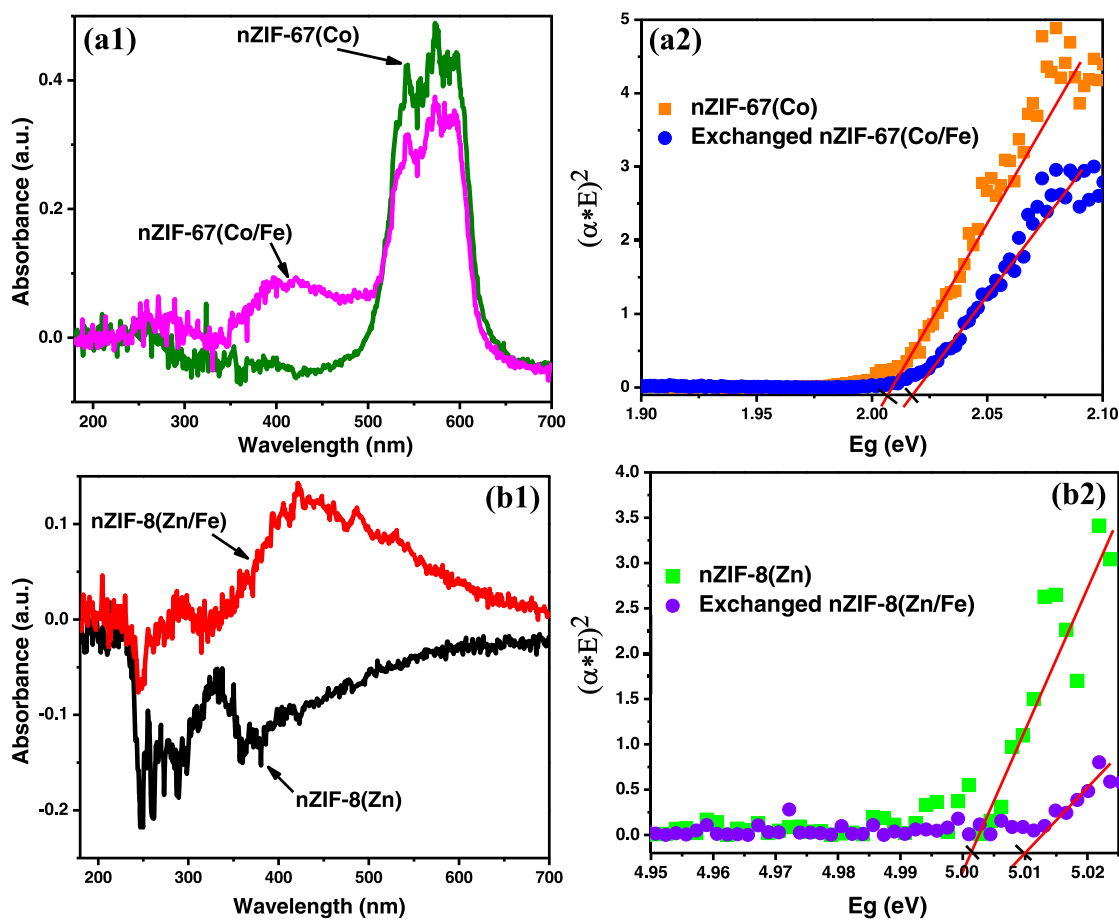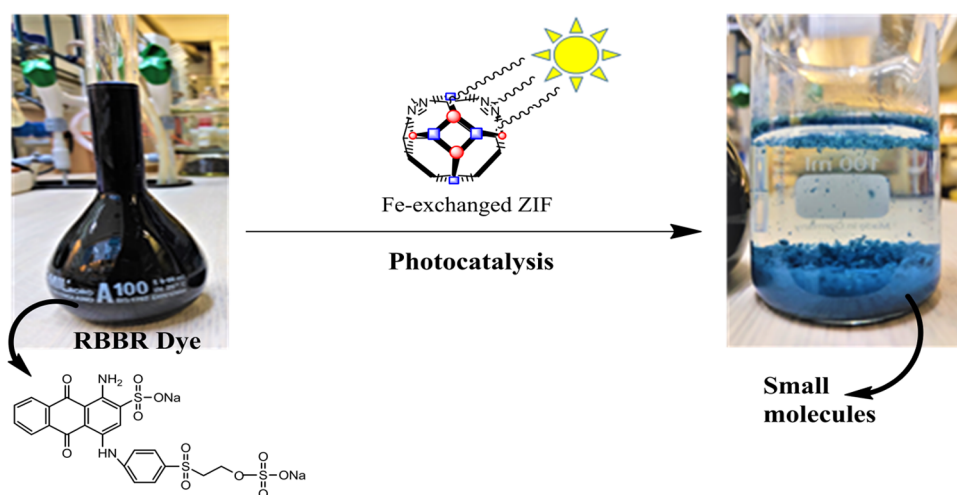
Figure 7. UV−vis spectra and the Tauc's plots of (a1, a2) nZIF-67(Co) with nZIF-67(Co/Fe) and (b1, b2) nZIF-8(Zn) with nZIF-8(Zn/Fe).

Scheme 1. Model of Photocatalytic Reaction of RBBR Dye on Fe-Exchanged ZIF Catalyst under Simulated Sunlight Illumination

light irradiation without the use of a catalyst, showed no signs of decomposition (Figure 8). This is in line with the literature.[26,37−43] Dark experiments were conducted in the presence of catalyst but without light irradiation. After 120 min (dark tests), the RBBR dye adsorptive concentration ratio (C/C_o) for parent ZIFs decreased by 50% (nZIF-8) and 40% (nZIF-67), respectively, but only 30% (nZIF-8(Zn/Fe)) and 20% (nZIF-67(Co/Fe)) for Fe-exchanged ZIFs. This low adsorptive removal of RBBR dye by Fe-exchanged ZIF

materials could be attributed to a decrease in the BET pore volume (Figure 5), which allowed fewer dye molecules to enter the pores. Under irradiation, the RBBR dye removal ability of the parent nZIF-8 (60%) and nZIF-67 (50%) only improved marginally. This suggests that RBBR degradation was primarily due to adsorption, and nZIF-8, similar to nZIF-67, lacked significant photocatalytic activity, which is similar to what was reported by Thanh et al.[26]
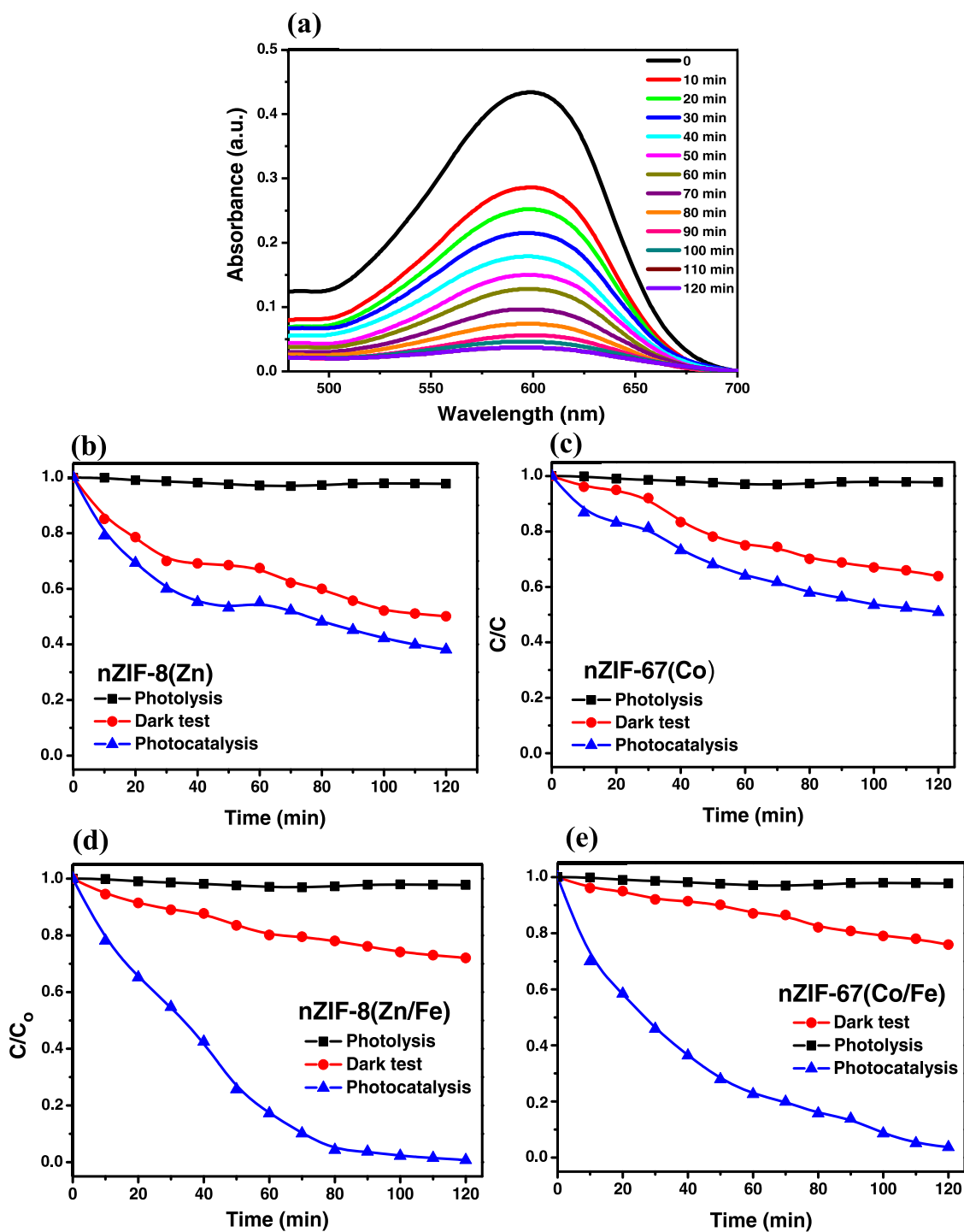
Figure 8. (a) UV−vis absorption spectra of the RBBR solution during decomposition reaction, and kinetics of photocatalytic degradation of RBBR by (b) nZIF-8(Zn), (c) nZIF-67(Co), (d) nZIF-8(Zn/Fe), and (e) nZIF-67(Co/Fe) under different conditions: in the dark with catalyst (●), without catalyst under irradiation (■), and with catalyst under irradiation (▲). Initial RBBR concentration = 20 mg dm^{-3}, catalyst loading = 50 mg, solution pH = 7.0, irradiation = 350 W metal halide lamp, and λ_{max} of RBBR = 595 nm.

Under irradiation, Fe-exchanged ZIFs demonstrate a remarkable photocatalytic degradation efficiency of RBBR dye. Photocatalytic decolorization fraction (C/C_o) decreased progressively and reaching 95% (nZIF-67(Co/Fe)) and 98% (nZIF-8(Zn/Fe)) after 120 min. It is certain that visible light irradiation and incorporation of Fe^{2+} into the ZIF framework improved the rate of dye degradation dramatically when compared to the dark test. Thus, the incorporation of Fe^{2+} into the ZIF framework enhances their photocatalytic activity and

removal efficiency of RBBR dye. The increase in dye degradation rate could be attributed to an increase in the number of active sites on the photocatalyst surface with more Fe^{2+} exposed. As a result, the number of photogenerated electron−hole pairs increased, resulting in a rise in the number of hydroxyl radicals responsible for dye degradation.[26,37−43] Electron−hole pairs can be formed using both light and a catalyst, resulting in the formation of oxidizing agents for the decomposition of organic pollutants, as seen with the high
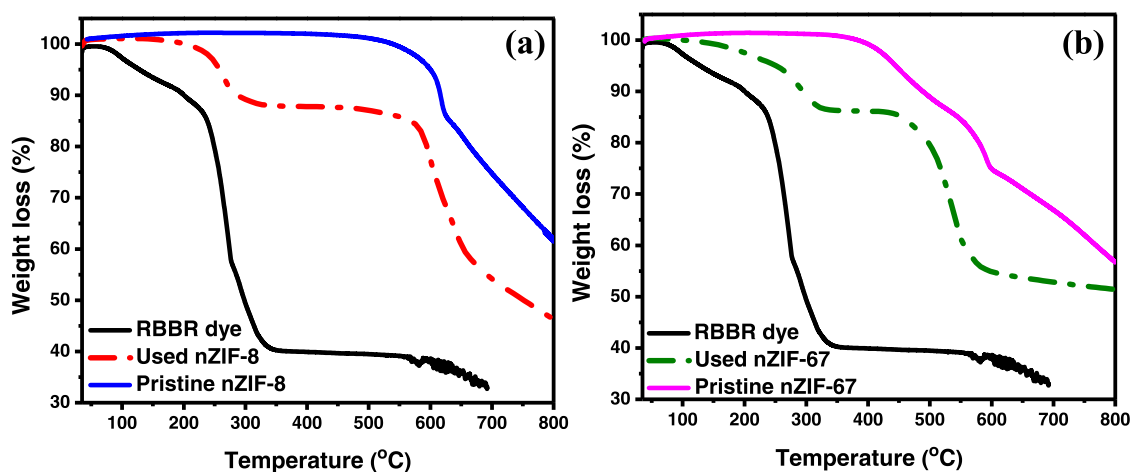
Figure 9. TGA thermograms of RBBR dye, pristine, and used (a) nZIF-8(Zn) and (b) nZIF-67(Co) after dark adsorption of RBBR dye.

RBBR dye degradation efficiency. After dark adsorption, TGA was utilized to confirm the presence of adsorbed RBBR dye in ZIF materials (Figure 9), which demonstrated a two-step thermal degradation of the employed ZIFs after 120 min. The first decomposition step occurred at 300 °C, which was comparable to the RBBR dye decomposition temperature, demonstrating the existence of adsorbed RBBR dye in both ZIF materials.

The first-order photocatalytic decolorization rate constant (K_{obs}) (Table 4 and Figure S6) showed that the fastest degradation was achieved by the Fe-exchanged ZIFs, nZIF-8(Zn/Fe) (2.20×10^{-2} min^{-1}) and nZIF-67(Co/Fe) (2.01×10^{-2} min^{-1}).

Table 4. K_{obs} and $T_{1/2}$ for nZIF-8, nZIF-67, and Their Fe-Exchanged Derivatives on the Photocatalytic Degradation of 20 mg dm^{-3} RBBR Dye

sample	K_{obs} (min^{-1})	$T_{1/2}$ (min)
nZIF-8(Zn)	1.19×10^{-2}	58.74
nZIF-67(Co)	5.59×10^{-3}	123.77
exchanged nZIF-8(Zn/Fe)	2.20×10^{-2}	31.51
exchanged nZIF-67(Co/Fe)	2.01×10^{-2}	34.48

FTIR of the RBBR dye degradation product showed that the major functional groups missing, compared to that of the original RBBR dye, were N−H (stretching vibration at 3420 cm^{-1}, (i) Figure 10) and N−C≡C (stretching vibration at 2224 cm^{-1}, (ii) Figure 10). This suggests that the product is most probably "1" (as seen in Scheme 2) in literature pathways for RBBR dye degradation.[45] Product 1 has no N−H and N−C bonds present. Pathway "2" (Scheme 2) results in products with amino groups and a hydroxyl group present. As the stretching vibrations of these groups were not observed by FTIR, the formation of product 2 can be ruled out.

3.2. Stability and Reusability. To determine the reusability of the Fe-exchanged ZIFs for the photocatalytic application, the nZIF-8(Zn/Fe) and nZIF-67(Co/Fe) used were regenerated by centrifuging with H$_2$O and followed by MeOH until the supernatant was colorless, dried for 12 h at 60 °C, and then activated at 150 °C under vacuum overnight before being reused for photocatalytic degradation of RBBR dye. The photocatalytic activity of the regenerated Fe-exchanged ZIFs only decreased marginally (less than 10%)
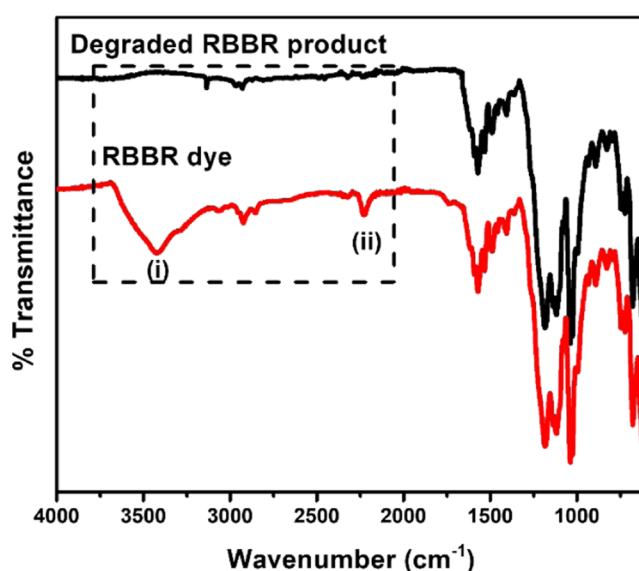

Figure 10. FTIR spectra of RBBR dye (red) and its degraded product (black).

after three cycles (Figure 11). The regenerated ZIF catalysts still performed well in terms of photocatalytic activity. The crystallinity of the Fe-exchanged ZIF catalysts as shown by their PXRD patterns (Figure 12) was retained after three photocatalytic cycles.

4. CONCLUSIONS

The Zn and Co nodes of nanosized ZIF-8(Zn) and ZIF-67(Co) were partially replaced by Fe(II), introduced by a one-step metal exchange to give the first bimetallic metal-exchanged microporous Fe(II)-containing ZIFs, nZIF-8(Zn/Fe) and nZIF-67(Co/Fe). A remarkably higher catalytic activity was observed for the photocatalytic degradation of textile dye (RBBR) by the Fe-exchanged nZIF-8 and nZIF-67 compared to their parent ZIFs. The incorporation of Fe(II) centers into the ZIF framework improved the photocatalytic activity of the framework dramatically by more than 50% for both nZIF-8 and nZIF-67. In addition, these catalysts can be regenerated and reused without appreciable loss in activity (Figure 12).

Scheme 2. Possible Products for Remazol Brilliant Blue R Degradation[*a*]
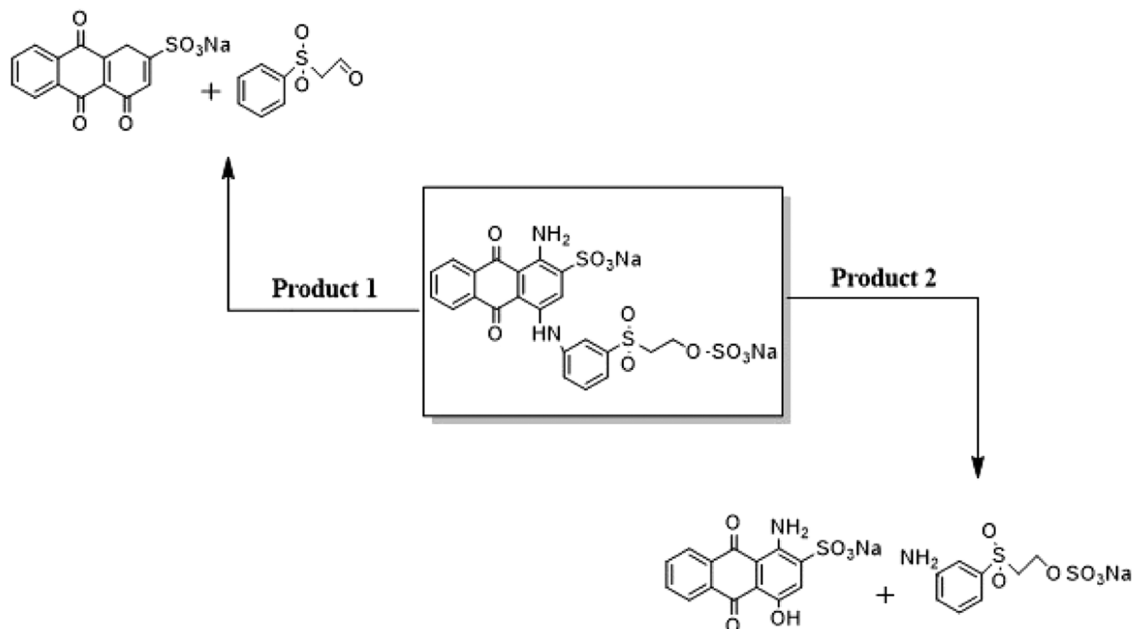
[*a*]Adapted with permission from [OSMA, J.F., TOCA HERRERA, J.L., RODRÍGUEZ COUTO, S. Transformation pathway of Remazol Brilliant Blue R by immobilised laccase. *Bioresour. Technol.*, **2010**, 101, 8509–8514. Doi: 10.1016/j.biortech.2010.06.074]. Copyright [2010] [Elsevier].[46]
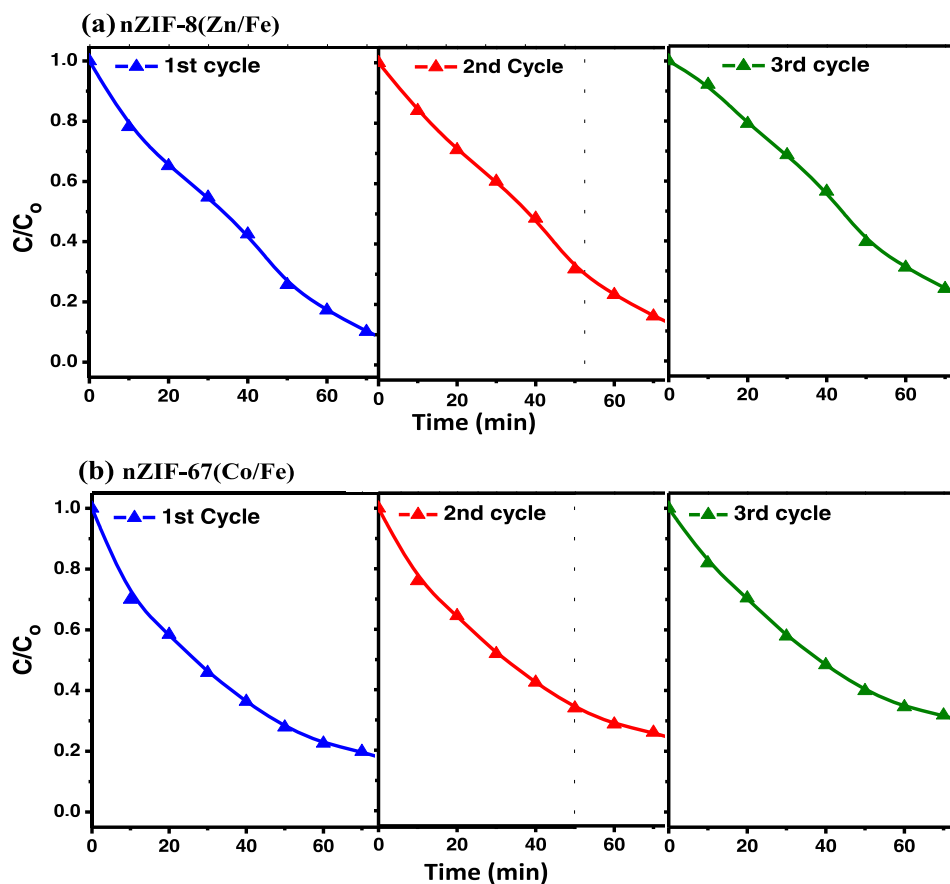

Figure 11. RBBR dye degradation by (a) nZIF-8(Zn/Fe) and (b) nZIF-67(Co/Fe) catalysts after the three photocatalytic cycles (mass of catalyst: 50 mg/100 cm^3, initial dye concentrations: 20 mg dm^{-3}).
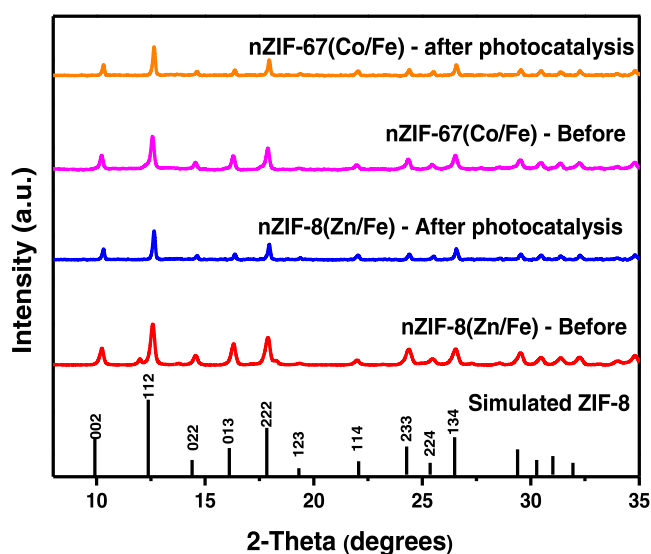
Figure 12. PXRD patterns of nZIF-8(Zn/Fe) and nZIF-67(Co/Fe) catalysts after the three photocatalytic cycles of degradation of RBBR dye.

5. EXPERIMENTAL SECTION

5.1. Materials and Equipment. Starting materials and solvents were purchased from Sigma-Aldrich and Merck with high purity and used without further purification, except where stated otherwise. A Bruker Tensor 27 infrared spectrophotometer equipped with a Pike Miracle single diamond attenuated total reflectance (ATR) crystal was used to measure all infrared spectra. A JSM-7800F Extreme-Resolution Analytical Field Emission scanning electron microscope fitted with an Oxford XMax (80 mm^2) energy-dispersive microscope was used to examine and analyze the SEM specimens. A Micromeritics ASAP 2020 surface area and porosity analyzer was used to measure the porosity and surface area up to 1 atm, and the data was analyzed using ASAP 2020 V2.0 and microactive software for physisorption. Prior to porosity measurements, the nano-ZIF materials were activated at 150 °C for 16 h, and a standard amount of ∼40 mg was used for each analysis, with warm and cold free space calculated separately. PXRD was collected at room temperature on a Bruker D2 Phaser powder X-ray diffractometer with a flat plate sample holder and Cu radiation (λ = 1.54 Å).[25] TGA was carried out on Mettler-Toledo TGA/SDTA851 in a nitrogen atmosphere at a heating rate of 10 °C·min^{-1} from 30 to 800 °C. With a monochromatic Al Kα X-ray source, XPS was recorded on a PHI 5000 Versaprobe system. The XPS data was analyzed with Multipak version 9.7c software, and Gaussian–

Lorentz fits were used (the Gaussian/Lorentz ratios were always >95%).[26,32]

5.2. Synthesis of Nano-ZIF-8(Zn) in Methanol.[27] Zn(NO$_3$)$_2$·6H$_2$O (1.297 g, 10 mmol) and 2-methylimidazole (3.306 g, 50 mmol) were dissolved separately in 50 cm^3 methanol (Scheme 3). The two solutions were mixed and stirred vigorously for 1 h at room temperature. The precipitate was isolated by centrifugation (8000 rpm, 15 min, 15 °C), washed with methanol (3 × 30 cm^3), and isolated by centrifugation. The solid white precipitate was left to dry and then activated at 150 °C for 12 h under vacuum to obtain nZIF-8(Zn). Yield: 0.827 g, 63%. νmax/cm^{-1} (Figure 2): ν(C=N) = 1589, ν(C–N) = 1151; 1039, ν(C–H) = 2930; 3138. PXRD (Figure 1).

5.3. Synthesis of Nano-ZIF-8(Zn) in Water.[28] Zn-(NO$_3$)$_2$·6H$_2$O (1.455 g, 10 mmol) and 2-methylimidazole (3.275 g, 50 mmol) were dissolved separately in 50 cm^3 deionized water (Scheme 3). TEA (5 cm^3) was added to the 2-methylimidazole solution, and then both solutions were mixed and stirred vigorously for 1 h at room temperature. The precipitate was isolated by centrifugation (8000 rpm, 15 min, 15 °C) and washed with deionized water (2 × 30 cm^3) and methanol (2 × 30 cm^3). Finally, the product was left to dry and then activated at 150 °C for 12 h under vacuum to obtain nZIF-8(Zn). Yield: 2.724 g, 94%. νmax/cm^{-1} (Figure 2): ν(C=N) = 1589, ν(C–N) = 1151; 1039, ν(C–H) = 2930; 3138. PXRD (Figure 1).

5.4. Surfactant-Mediated Synthesis of Nano-ZIF-67(Co) in Methanol or Water.[29,30] A surfactant (0.5 g; PVP-10) and TEA (5 cm^3) were sonicated for 5 min in 50 cm^3 methanol or deionized water to give a homogeneous aqueous solution (Scheme 4). 2-Methylimidazole (3.275 g, 50 mmol) was added to the solution, followed by another 5 min of sonication. Co(NO$_3$)$_2$·6H$_2$O (1.455 g, 10 mmol) was dissolved in 50 cm^3 methanol or deionized water. The two solutions were mixed and stirred vigorously for 1 h at room temperature. The precipitate was isolated by centrifugation (8000 rpm, 15 min, 15 °C), washed with methanol (3 × 50 cm^3), and isolated by centrifugation. The solid purple precipitate was left to dry and then activated at 150 °C for 12 h under vacuum to obtain nZIF-67(Co). Yields: (1.572 g, 61% for MeOH) and (2.413 g, 93% for H$_2$O). νmax/cm^{-1} (Figure 2): ν(C=N) = 1589, ν(CN) = 1151; 1039, ν(C–H) = 2930; 3138. PXRD (Figure 1).

5.5. Metal-Ion Exchange between ZIFs and Fe(acac)$_2$. Fe-exchanged ZIF materials were synthesized by modifying the procedure described by Song et al. (Scheme 5).[25] All reagents were mixed in a glovebox to avoid oxidation of Fe(II). Fe(acac)$_2$ (1.50 g, 6 mmol) was dissolved in 50 cm^3 methanol

Scheme 3. Isothermal Synthesis of ZIF-8 Nanoparticles from Zinc Nitrate Hexahydrate and 2-Methylimidazole
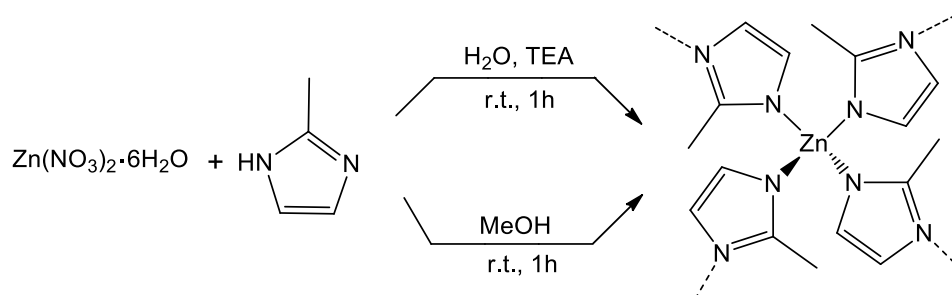
Scheme 4. Surfactant-Mediated Synthesis of ZIF-67 Nanoparticles from Cobalt Nitrate Hexahydrate and 2-Methylimidazole
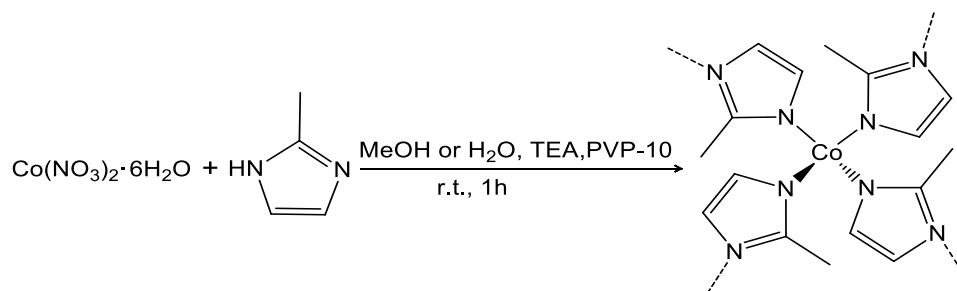
Scheme 5. Fe(II)-Exchange of ZIF-8(Zn) and ZIF-67(Co) Nanoparticles

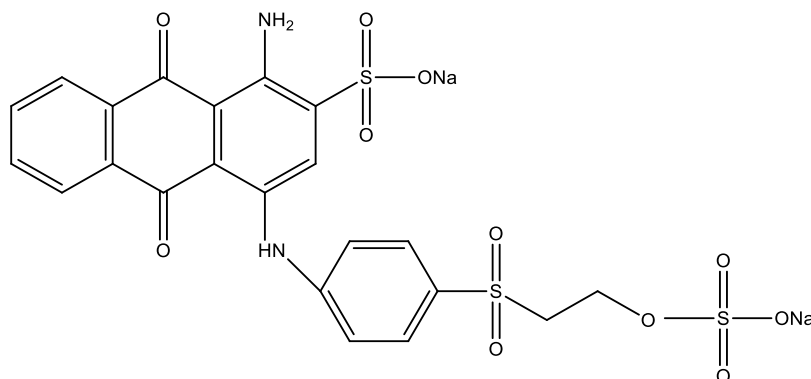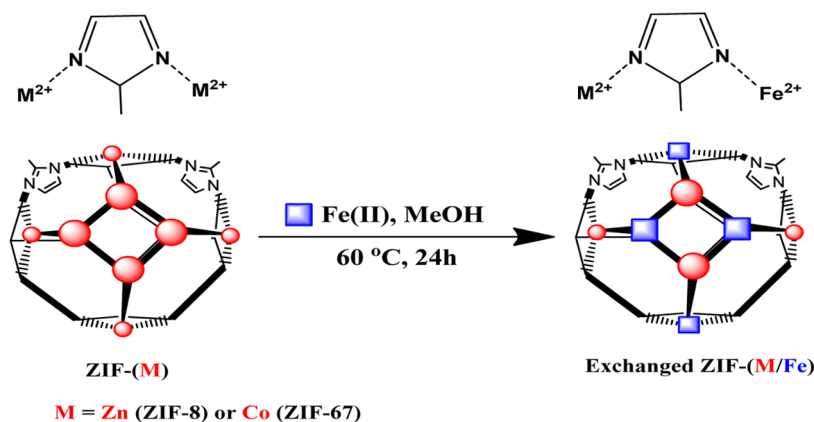**Figure 13.** Molecular structure of Remazol Brilliant Blue R (RBBR).

using an ultrasonic bath. This solution was added to the solution containing $Zn(NO_3)_2 \cdot 6H_2O$ and 2-methylimidazole for ZIF-8 and $Co(NO_3)_2 \cdot 6H_2O$ and 2-methylimidazole for ZIF-67. The mixture was refluxed at 60 °C for 24 h under N_2. After cooling to room temperature, the mixture was centrifuged (8000 rpm, 15 min, 15 °C). The precipitate was washed with $(3 \times 30 \text{ cm}^3)$ methanol. The solids were left to soak in methanol for 3 days, and the solution was exchanged with fresh methanol every 24 h. The solids were centrifuged until the supernatant was colorless and dried at 80 °C.

5.6. Photocatalytic Application (RBBR Dye Degradation). The photocatalytic activities of metal-exchanged nZIF-8(Zn/Fe) and nZIF-67(Co/Fe), compared to their parents nZIF-8 (Zn) and nZIF-67(Co), were studied in the degradation of Remazol Brilliant Blue R (RBBR) dye (Figure 11) under simulated sunlight irradiation using a 350 W Metal Halide Lamp in an open air at room temperature. Both dark adsorption and photocatalytic degradation reactions were

carried out to differentiate between the adsorption and photocatalytic degradation of the generated catalysts. Adsorption experiments were performed in the dark, while photocatalytic tests were performed with light irradiation. Fifty milligrams of the ZIF catalyst was placed in a 250 cm^3 beaker containing 100 cm^3 of dye solution (20 mg dm^{-3}, pH = 7.0), which were stirred magnetically. Five cubic centimeters of the samples was taken at 10 min time intervals, and the RBBR concentration was measured using a Shimadzu CPS-240A UV−vis spectrophotometer, corresponding to λ_{max} of dye = 595 nm (Figure 13).

■ ASSOCIATED CONTENT

ⓢ Supporting Information

The Supporting Information is available free of charge at https://pubs.acs.org/doi/10.1021/acsomega.1c04142.

> SEM images; EDS spectra and mapping; particle size distribution; stability FTIR and XPS spectra; and UV−

vis spectra and first-order kinetic curves of dye degradation (PDF)

■ AUTHOR INFORMATION

Corresponding Author

　Ernst H. G. Langner − *Department of Chemistry, University of the Free State, Bloemfontein 9300, South Africa;* ⊙ orcid.org/0000-0002-4667-3396; Email: langneeh@ufs.ac.za

Authors

　Lehlohonolo E. Mphuthi − *Department of Chemistry, University of the Free State, Bloemfontein 9300, South Africa;* ⊙ orcid.org/0000-0003-1433-1903

　Elizabeth Erasmus − *Department of Chemistry, University of the Free State, Bloemfontein 9300, South Africa;* ⊙ orcid.org/0000-0003-0546-697X

Complete contact information is available at:
https://pubs.acs.org/10.1021/acsomega.1c04142

Notes

The authors declare no competing financial interest.

■ REFERENCES

(1) Corma, A. From microporous to mesoporous molecular sieve materials and their use in catalysis. *Chem. Rev.* **1997**, *97*, 2373−2420.

(2) Chen, B.; Yang, Z.; Zhu, Y.; Xia, Y. Zeolitic imidazolate framework materials: recent progress in synthesis and applications. *J. Mater. Chem. A* **2014**, *2*, 16811−16831.

(3) Eddaoudi, M.; Sava, D. F.; Eubank, J. F.; Adil, K.; Guillerm, V. Zeolite-like metal organic frameworks (ZMOFs): design, synthesis, and properties. *Chem. Soc. Rev.* **2015**, *44*, 228−249.

(4) Shi, F. N.; Rosero-Navarro, N. C.; Barbosa, P.; Figueiredo, F. M. Protonic Conductivity of Nanocrystalline Zeolitic Imidazolate Framework 8. *Electrochim. Acta* **2015**, *153*, 19−27.

(5) Liu, Y.; Pang, H.; Wang, X.; Yu, S.; Chen, Z.; Zhang, P.; Chen, L.; Song, G.; Saleh Alharbi, N.; Omar Rabah, S.; Wang, X. Zeolitic imidazolate framework-based nanomaterials for the capture of heavy metal ions and radionuclides: A review. *Chem. Eng. J.* **2021**, *406*, No. 127139.

(6) Ranocchiari, M.; van Bokhoven, J. A. Catalysis by metal-organic frameworks: fundamentals and opportunities. *Phys. Chem. Chem. Phys.* **2011**, *13*, 6388−6396.

(7) Zhou, H.; Long, J. R.; Yaghi, O. M. Introduction to Metal−Organic Frameworks. *Chem. Rev.* **2012**, *112*, 673−674.

(8) Biswas, S.; Stock, N. Synthesis of metal-organic frameworks (MOFs): routes to various MOF topologies, morphologies, and composites. *Chem. Rev.* **2012**, *112*, 933−969.

(9) Deneff, J. I.; Butler, K. S.; Kotula, P. G.; Rue, B. E.; Sava Gallis, D. F. Expanding the ZIFs Repertoire for Biological Applications with the Targeted Synthesis of ZIF-20 Nanoparticles. *ACS Appl. Mater. Interfaces* **2021**, *13*, 27295−27304.

(10) Jian, M.; Liu, B.; Liu, R.; Qu, J.; Wang, H.; Zhang, X. Water-based synthesis of zeolitic imidazolate framework-8 with high morphology level at room temperature. *RSC Adv.* **2015**, *5*, 48433−48441.

(11) Venna, S. R.; Jasinski, J. B.; Carreon, M. A. Structural evolution of zeolitic imidazolate framework-8. *J. Am. Chem. Soc.* **2010**, *132*, 18030−18033.

(12) Tanaka, S.; Kida, K.; Okita, M.; Ito, Y.; Miyake, Y. Size-controlled Synthesis of Zeolitic Imidazolate Framework-8 (ZIF-8) Crystals in an Aqueous System at Room Temperature. *Chem. Lett.* **2012**, *41*, 1337−1339.

(13) Zaręba, J.; Nyk, M.; Samoć, M. Co/ZIF-8 Heterometallic Nanoparticles: Control of Nanocrystal Size and Properties by a Mixed-Metal Approach. *Cryst. Growth Des.* **2016**, *16*, 6419−6425.

(14) Sun, W.; Zhai, X.; Zhao, L. Synthesis of ZIF-8 and ZIF-67 nanocrystals with well-controllable size distribution through reverse microemulsions. *Chem. Eng. J.* **2016**, *289*, 59−64.

(15) Horike, S.; Kadota, K.; Itakura, T.; Inukai, M.; Kitagawa, S. Synthesis of magnesium ZIF-8 from $Mg(BH_4)_2$. *Dalton Trans.* **2015**, *44*, 15107−15110.

(16) Tian, Y. Q.; Yao, S. Y.; Gu, D.; Cui, K. H.; Guo, D. W.; Zhang, G.; Chen, Z. X.; Zhao, D. Y. Cadmium imidazolate frameworks with polymorphism, high thermal stability, and a large surface area. *Chem. - Eur. J.* **2010**, *16*, 1137−1141.

(17) Kadota, K.; Sivaniah, E.; Bureekaew, S.; Kitagawa, S.; Horike, S. Synthesis of manganese ZIF-8 from $[Mn(BH4)_2 \cdot 3THF] \cdot NaBH_4$. *Inorg. Chem.* **2017**, *56*, 8744−8747.

(18) López-Cabrelles, J.; Romero, J.; Abellán, G.; Giménez-Marqué, M.; Palomino, M.; Valencia, S.; Rey, F.; Espallargas, G. Solvent-Free Synthesis of ZIFs: A Route toward the Elusive Fe(II) Analogue of ZIF-8. *J. Am. Chem. Soc.* **2019**, *141*, 7173−7180.

(19) Zanon, A.; Verpoort, F. Metals@ZIFs: Catalytic applications and size selective catalysis. *Coord. Chem. Rev.* **2017**, *353*, 201−222.

(20) Liu, Y.; Cheng, H.; Cheng, M.; Liu, Z.; Huang, D.; Zhang, G.; Shao, B.; Liang, Q.; Luo, S.; Wu, T.; Xiao, S. The application of Zeolitic imidazolate frameworks (ZIFs) and their derivatives based materials for photocatalytic hydrogen evolution and pollutants treatment. *Chem. Eng. J.* **2021**, *417*, No. 127914.

(21) Kalaj, M.; Cohen, S. M. Postsynthetic Modification: An Enabling Technology for the Advancement of Metal−Organic Frameworks. *ACS Cent. Sci.* **2020**, *6*, 1046−1057.

(22) Tanabe, K. K.; Cohen, S. M. Postsynthetic modification of metal−organic frameworks-a progress report. *Chem. Soc. Rev.* **2011**, *40*, 498−519.

(23) Kim, M.; Cahill, J.; Fei, H.; Prather, K.; Cohen, S. Postsynthetic Ligand and Cation Exchange in Robust Metal−Organic Frameworks. *J. Am. Chem. Soc.* **2012**, *134*, 18082−18088.

(24) Deria, P.; Mondloch, E.; Karagiaridi, O.; Bury, W.; Hupp, T.; Farha, K. Beyond post-synthesis modification: evolution of metal−organic frameworks via building block replacement. *Chem. Soc. Rev.* **2014**, *43*, 5896−5912.

(25) Song, F.; Cao, Y.; Zhao, Y.; Jiang, R.; Xu, Q.; Yan, J.; Zhong, Q. Ion-Exchanged ZIF-67 Synthesized by One-Step Method for Enhancement of CO2 Adsorption. *J. Nanomater.* **2020**, *2020*, No. 1508574.

(26) Thanh, M.; Thien, T.; Du, P.; Hung, N.; Khieu, D. Iron doped zeolitic imidazolate framework (Fe-ZIF-8): synthesis and photocatalytic degradation of RDB dye in Fe-ZIF-8. *J. Porous Mater.* **2018**, *25*, 857−869.

(27) Tsai, C.; Niemantsverdriet, J. W.; Langner, E. H. G. Enhanced CO2 adsorption in nano-ZIF-8 modified by solvent assisted ligand Exchange. *Microporous Mesoporous Mater.* **2018**, *262*, 98−105.

(28) Khan, I. U.; Othman, M. H. D.; Jilani, A.; Ismail, A. F.; Hashim, H.; Jaafar, J.; Rahman, M. A.; Rehman, G. U. Economical, environmental friendly synthesis, characterization for the production of zeolitic imidazolate framework-8 (ZIF-8) nanoparticles with enhanced CO2 adsorption. *Arabian J. Chem.* **2018**, *11*, 1072−1083.

(29) Fan, X.; Wang, W.; Li, W.; Zhou, J.; Wang, B.; Zheng, J.; Li, X. Highly Porous ZIF-8 nanocrystals Prepared by a Surfactant Mediated Method in Aqueous Solution with Enhanced Adsorption Kinetics. *ACS Appl. Mater. Interfaces* **2014**, *6*, 14994−14999.

(30) Li, Y.; Zhou, K.; He, M.; Yao, J. Synthesis of ZIF-8 and ZIF-67 using mixed-base and their dye adsorption. *Microporous Mesoporous Mater.* **2016**, *234*, 287−292.

(31) Fei, H.; Cahill, J.; Prather, K.; Cohen, S. Tandem Postsynthetic Metal Ion and Ligand Exchange in Zeolitic Imidazolate Frameworks. *Inorg. Chem.* **2013**, *52*, 4011−4016.

(32) Moulder, F.; Stickle, W. F.; Sobol, P. E.; Bomben, K. D. *Handbook of X-ray Photoelectron Spectroscopy*; ULVAC-PHI, Inc.: Enzo, Chigasaki, Japan, 1995.

(33) Hamid, M. R. A.; Park, S.; Kim, J. S.; Lee, Y. M.; Jeong, H. In-Situ Formation of Zeolitic-Imidazolate Framework Thin Films and Composites Using Modified Polymer Substrates. *J. Mater. Chem. A* **2019**, *7*, 9680−9689.

(34) Nqombolo, A.; Munonde, T. S.; Makhetha, T. A.; Moutloali, R. M.; Nomngongo, P. N. Cobalt/zinc-based metal organic frameworks as an effective adsorbent for improved removal of As(V) and Cr(VI) in a wide pH range. *J. Mater. Res. Technol.* **2021**, *12*, 1845−1855.

(35) Wu, W.; Su, J.; Jia, M.; Li, Z.; Liu, G.; Li, W. Vapor-phase linker exchange of metal-organic frameworks. *Sci. Adv.* **2020**, *6*, No. 7270.

(36) Bhatt, B.; et al. Biological decolorization of the synthetic dye RBBR in contaminated soil. *World J. Microbiol. Biotechnol.* **2000**, *16*, 195−198.

(37) Chang, S.; Chuang, S.; Li, H.; Liang, H.; Huang, L. Comparative study on the degradation of I.C. Remazol Brilliant Blue R and I.C. Acid Black 1 by Fenton oxidation and Fe^0/air process and toxicity evaluation. *J. Hazard. Mater.* **2009**, *166*, 1279−1288.

(38) Algubili, A. M.; Alrobayi, E. M.; Alkaim, A. F. Photocatalytic degradation of Remazol Brilliant Blue Dye by ZnO/UV Process. *Int. J. Chem. Sci.* **2015**, *13*, 911−921.

(39) Lei, X.; Cao, Y.; Chen, Q.; Ao, X.; Fang, Y. B.; Liu, Y. ZIF-8 derived hollow CuO/ZnO material for study of enhanced photo-catalytic performance. *Colloids Surf., A* **2019**, *568*, 1−10.

(40) Amini, M.; Ashrafi, M. Photocatalytic degradation of some organic dyes under solar light irradiation using TiO$_2$ and ZnO nanoparticles. *Nanochem. Res.* **2016**, *1*, 79−86.

(41) Pan, D.; Ge, S.; Zhao, J.; Tian, J.; Shao, Q.; Guo, L.; Mai, X.; Wu, T.; Murugadoss, V.; Liu, H.; Ding, T.; Angaiah, S.; Guo, Z. Synthesis and Characterization of ZnNiIn Layered Double Hydrox-ides Derived Mixed Metal Oxides with Highly Efficient. Photo-electrocatalytic Activities. *Ind. Eng. Chem. Res.* **2019**, *58*, 836−848.

(42) Abdi, J. Synthesis of Ag-doped ZIF-8 photocatalyst with excellent performance for dye degradation and antibacterial activity. *Colloids Surf., A* **2020**, *604*, No. 125330.

(43) Ökte, A. N.; Karamanis, D.; Chalkia, E.; Tuncel, D. The effect of ZnO or TiO2 loaded nanoparticles on the adsorption and photocatalytic performance of Cu-BTC and ZIF-8 MOFs. *Mater. Chem. Phys.* **2017**, *187*, 5−10.

(44) Saliba, D.; Ammar, M.; Rammal, M.; Al-Ghoul, M.; Hmadeh, M. Crystal Growth of ZIF-8, ZIF-67, and Their Mixed-Metal Derivatives. *J. Am. Chem. Soc.* **2018**, *140*, 1812−1823.

(45) Legerská, B.; Chmelová, D.; Ondrejovič, M. Degradation of Synthetic Dyes by Laccases—A Mini-Review. *Nova Biotechnol. Chim.* **2016**, *15*, 90−106.

(46) Osma, J. F.; Toca Herrera, J. L.; Rodríguez Couto, S. Transformation pathway of Remazol Brilliant Blue R by immobilised laccase. *Bioresour. Technol.* **2010**, *101*, 8509−8514.